Mem. S.A.It. Vol. 86, 236

Memorie della

On the He burning phases of the Carina dSph

M. Fabrizio[1], A. Pietrinferni[1], G. Bono[2,3], P.B. Stetson[4], A.R. Walker[5], R. Buonanno[1,2], S. Cassisi[1], I. Ferraro[3], G. Iannicola[3], M. Monelli[6], M. Nonino[7], L. Pulone[3], and F. Thevénin[8]

[1] INAF–OATe, via M. Maggini – 64100, Teramo, Italy
[2] Univ. Rome "Tor Vergata", Via della Ricerca Scientifica, 1 – 00133, Roma, Italy
[3] INAF–OAR, via Frascati 33 – 00040, Monte Porzio Catone (RM), Italy
[4] DAO–HIA, NRC, 5071 West Saanich Road, Victoria, BC V9E 2E7, Canada
[5] NOAO–CTIO, Casilla 603, La Serena, Chile
[6] IAC, Calle Via Lactea, E38200 La Laguna, Tenerife, Spain
[7] INAF–OAT, via G.B. Tiepolo 11 – 34143, Trieste, Italy
[8] Obs. Côte d'Azur, BP 4229 – 06304, Nice, France

Abstract. We performed a detailed comparison between predicted He burning phases and multiband photometry of the Carina dwarf spheroidal galaxy. We found a good agreement with the predictions computed assuming an α-enhanced chemical mixture, indicating a mean metallicity [Fe/H] ~ -1.8 with a raw observed peak-to-peak spread in iron abundance of 0.4±0.2 dex.

Key words. Galaxies: individual (Carina) — Galaxies: dwarf — Local Group — Galaxies: stellar content — Galaxies: stellar content — Stars: evolution

1. Introduction

Dwarf galaxies and the newly discovered ultra-faint-dwarf galaxies are the crossroad of several theoretical and empirical investigations. The reasons are manifold. *a)* These relatively small stellar systems fix the limit beyond which the dark matter halos do not form stars. This means that their number and intrinsic properties can provide firm constraints on the timescale during which these subhalos have been accreted by their parent galaxies (Rocha et al. 2012, 2013), and in turn to validate current dark matter simulations of galaxy formation. *b)* Photometric and spectroscopic data indicate that dwarf galaxies do obey to a "linear" relation between metallicity and luminosity (see Fig. 7 in Mateo 1998). This evidence was originally brought forward by Skillman et al. (1989) and cover more than 3 dex in metallicity and ≈15 mag in luminosity. The above empirical evidence suggests that the chemical enrichment of these systems was mainly driven by internal mechanisms. However, we still lack firm constraints on the intrinsic metallicity dispersion and their possible correlation with intermediate-age and old stellar populations. *c)* The relevant number of dwarf galaxies recently discovered by the SDSS in the Local Group (McConnachie 2012) improved the observational basis of the so-called "density–morphology" relation. Empirical evidence indicates that dwarf galaxies located closer to the two giant galaxies (Milky Way, M31) are typically gas–poor, spherical and non rotating, while those located at larger distances are gas–rich, irregular and rotating (Grcevich & Putman 2009). Numerical simulations suggest that the morphology segregation might be explained as the consequence of both ram pressure stripping and tidal stirring: once field dwarf irregulars are accreted they will be transformed into dwarf spheroidals (dSphs, Łokas et al. 2010). However, the above scenario is hampered by the limited sample of spectroscopic data available for old tracers in nearby dwarf galaxies.

We present preliminary results on the mean metallicity of the stellar populations in the Carina dSph using multiband photometry.

2. Optical Color-Magnitude diagrams

We have already collected a large set (4152) of multi-band optical (U, B, V, I) images of the Carina dSph (Bono et al. 2010a; Stetson et al. 2011). The optical (V, $B-I$; V, $B-V$) Carina Color-Magnitude Diagram (CMD) has already been discussed in several investigations. On the basis of BV photometry Battaglia et al. (2012) found evidence of a spread in age, when moving from the innermost regions to regions located beyond the nominal truncation radius.

The advanced evolutionary properties of low- and intermediate-mass stars provide at least three independent metallicity indicators: *a)* the slope and the spread in color of the red giant branch (RGB); *b)* the spread in color of red clump (RC) stars; *c)* the zero-age-horizontal-branch (ZAHB) luminosity and the spread in magnitude of horizontal branch (HB) stars. The photometric analysis showed a very limited range in color covered by RGB and RC stars, as well as the spread in magnitude of blue and red HB stars[1]. The above evidence suggests that Carina stars cover a range in metallicity smaller than ~ 0.6 dex (Bono et al. 2010a).

A similar analysis was also performed by Stetson et al. (2011), but using stellar isochrones of different ages and chemical compositions. The theoretical framework they adopted for both scaled-solar and α-enhanced evolutionary models is based on isochrones available in the BaSTI[2] database (Pietrinferni et al. 2004, 2006). They found that both the old (12 Gyr) and the intermediate-age (4-6 Gyr) sub-populations show a limited spread in chemical composition. The above results support mean iron abundances ([Fe/H] $= -1.72$, $\sigma = 0.24$) based on high-resolution spectra for 44 RGs recently provided by Fabrizio et al. (2012, see also Lemasle et al. 2012 and Venn et al. 2012). Stellar populations in Carina were also investigated using synthetic CMDs and a new Bayesan approach by Small et al. (2013). They found that the 34% of the stars are old (13 Gyr), while the 46% are intermediate (4.5-7 Gyr), plus a plume of younger objects.

We discuss the evolutionary properties of the Carina sub-populations using HB stars are tracers of the old population and RC stars as tracers of the intermediate-age population.

The Fig. 1 shows the comparison between observations and theory, in the V, $B-V$ (left) and V, $B-I$ (right) CMD. To compare theory and observations we adopted the distance modulus and the reddening available in the literature (Monelli et al. 2003; Dall'Ora et al. 2003; Pietrzyński et al. 2009). The selective extinction coefficients that we adopted are the following: $R_V = 3.07$, $R_B = 4.07$ and $R_I = 1.65$ from McCall (2004, see also Bono et al. 2010b for further details). Candidate Carina stars were selected according to the $U-V$, $B-I$ color-color plane (Bono et al. 2010a). In the right panel, the 1379 stars with visual magnitudes brighter than 20.75 were selected according to kinematic properties (Fabrizio et al. 2011). The isochrones range from 2 (dashed-dotted-dotted) to 13 (dashed) Gyr. They have been computed assuming an iron abundance of [Fe/H] $= -1.79$ and a scaled-solar chemical mixture.

The precision of the photometric catalog allows us to constrain the properties of

[1] The off-ZAHB evolution also increases the spread in magnitude of HB stars. However, a detailed analysis of the pulsation properties of Carina RR Lyrae indicates that they are marginally affected by evolutionary effects (Coppola et al. 2013).

[2] `http://albione.oa-teramo.inaf.it/`

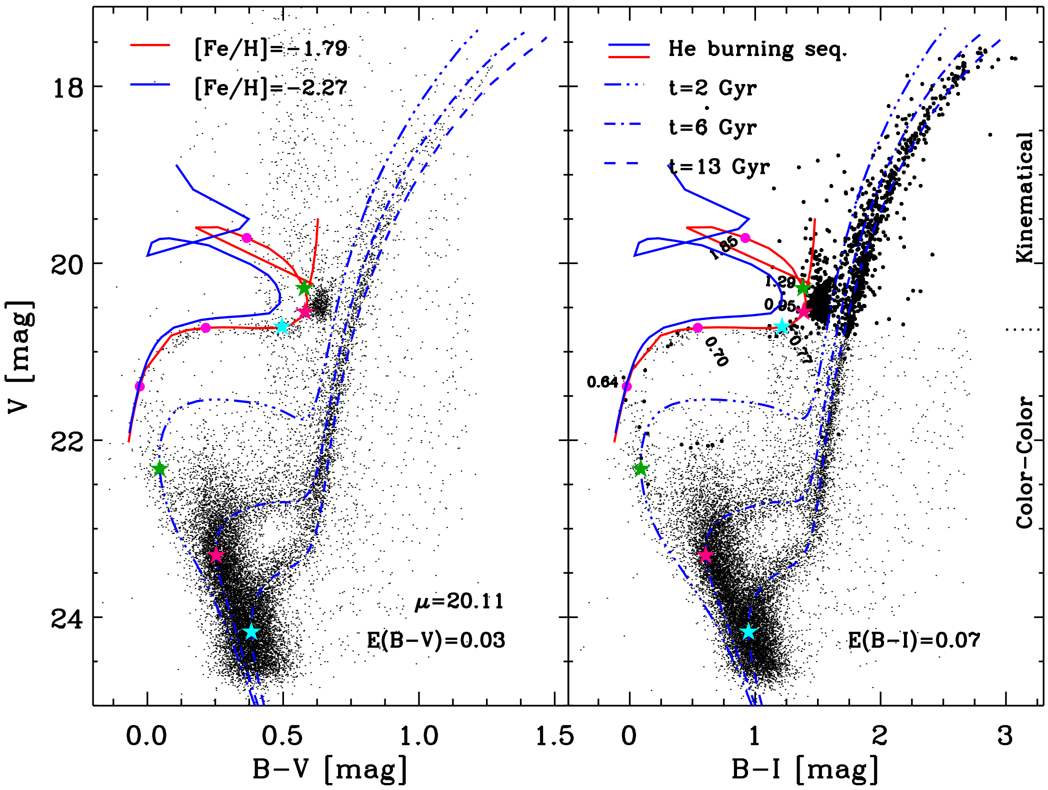

Fig. 1. Left – Comparison in the V, $B-V$ CMD between candidate Carina stars selected on the basis of the $U-V$, $B-I$ color-color plane (Bono et al. 2010a) and isochrones computed adopting a scaled-solar chemical composition ([Fe/H] = −1.79). The ages range from 2 (dashed-dotted-dotted) to 13 (dashed) Gyr. The solid blue and red lines show the predicted He burning sequences for two different iron abundances. The adopted true distance modulus and reddening are also labelled. Right – same as the left, but for the V, $B-I$ CMD. The 1379 stars with visual magnitudes brighter than 20.75 were selected according to kinematic properties (Fabrizio et al. 2011). The labels along the metal-poor He burning sequence display selected mass values (see text for details).

the different sub-populations for the old, the intermediate-age and the young stellar populations. The old population is well reproduced by an isochrone of 13 Gyr, this means a main sequence turn off (MSTO) mass value of $M = 0.77\ M_\odot$. An isochrone of 6 Gyr is a good average for the intermediate-age population, with a MSTO mass of $M = 0.95\ M_\odot$. Note that this star formation event shows evidence of a spread in age of the order of 2 Gyr. The blue plume (youngest stellar population) is well reproduced by a 2 Gyr isochrone (MSTO mass $M = 1.29\ M_\odot$), once again with an age spread. The BaSTI evolutionary tracks were computed assuming a Reimers mass loss rate ($\eta = 0.4$), this means that the stellar structures approaching the tip of the RGB (TRGB) will have smaller mass values: 0.69 (old), 0.89 (intermediate) and 1.25 (young) $M_\odot$. The relative difference is due to the fact that the RGB phase of the old population is significantly longer (440 Myr) when compared with the intermediate (250 Myr) and the young (120 Myr) stellar population. Indeed, low-mass stars develop an electron degenerate He core, and therefore, the He ignition (3α) is delayed until the He core mass approaches 0.5 $M_\odot$.

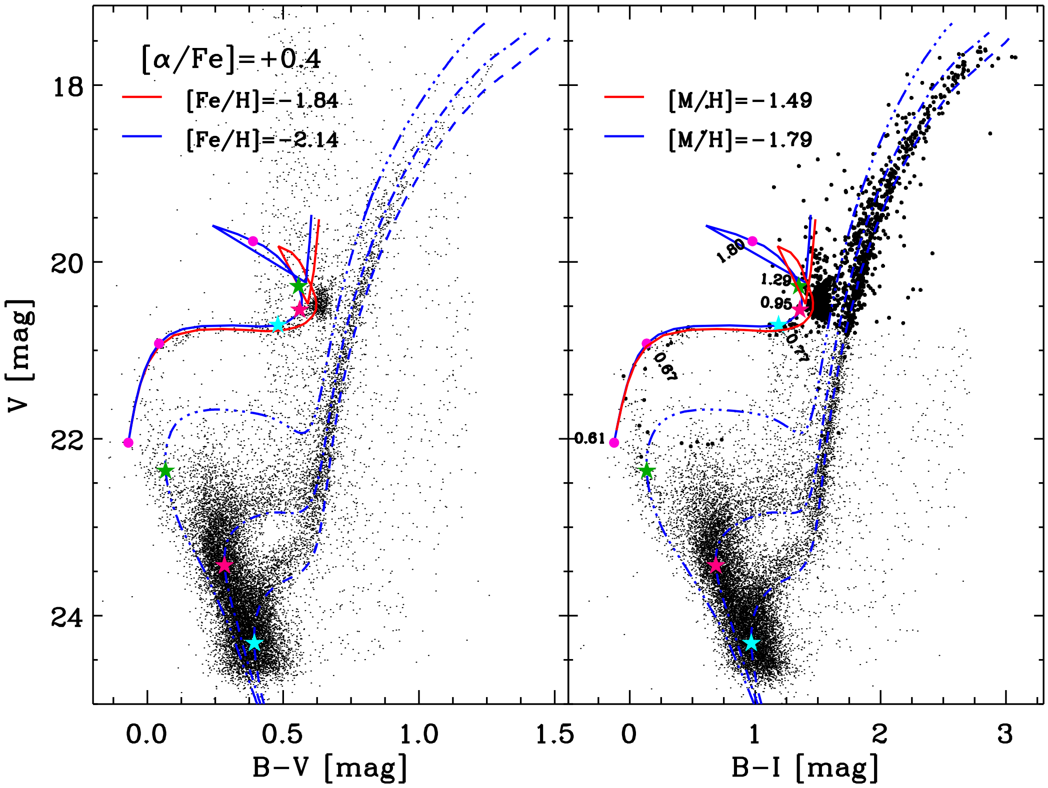

Fig. 2. Same as Fig. 1, but for isochrones and He burning sequences constructed assuming an α-enhanced chemical mixture. The iron abundances and the global metallicities [M/H] are also labelled.

The solid blue and red lines display predicted He burning sequences of old and intermediate-age progenitors for two different metal abundances (see labeled values). The ZAHB of the old population was computed[3] assuming an age for the progenitor of 13 Gyr, which means a mass value at the TRGB of 0.69 $M_\odot$. The position along the ZAHB of a structure with the mass value of the MSTO was marked with a cyan star. The above evolutionary scenario only accounts for "reddish" HB stars. However, empirical evidence indicates that the HB morphology ranges from extremely hot (≈35,000 K), less massive (0.55 $M_\odot$) to cool (≈5,000 K), more massive (0.80 $M_\odot$) HB stars. To account for this difference in HB morphology we assume that hot HB stars experienced a more efficient mass loss along the RGB. This assumption is supported by empirical evidence, suggesting that the mass-loss rate is far from being steady along the RGB (McDonald et al. 2011). To provide a more quantitative analysis of this phenomenon we also marked the ZAHB stellar structures with a mass of 0.64 and 0.70 $M_\odot$, i.e. structures that lost along the RGB the ∼17% and the ∼9% of their initial mass.

The intermediate-age He burning sequence (IAHBS) becomes brighter and slightly hotter. The change is mainly caused by the fact that in stellar structures more massive than ∼1.3 $M_\odot$ the He burning takes place in a He core that is only partially affected by electron degeneracy (RC). For these stellar structures, the decrease in He burning efficiency, due to the decrease in the He core mass, is superseded by

[3] The ZAHB V-magnitude was increased by 0.05 mag to account for the decrease in the He-core mass caused by the use of more updated conductive opacities (Cassisi et al. 2007).

the increased efficiency of the hydrogen burning shell. The magenta star marks along the IAHBS the position of the 6 Gyr stellar population. Stellar structures with slightly younger age show a trend similar to RC stars: they become steadily brighter and hotter (green star). A sharp change in this behavior takes place for $M \geq 2.0$ $M_{\odot}$ ($t \sim 600$ Myr), since they become suddenly fainter and cooler. Structures more massive than this limit undergo a quiescent He burning ignition at the tip of the RGB (Sweigart et al. 1989; Fiorentino et al. 2012). The He burning phase of even more massive structures develop, for the above abundance, the so-called blue loops (Bono et al. 2000). This scenario is supported by the identification in Carina of several Anomalous Cepheids associated to the RC phase and a few candidate short-period classical Cepheids, associated to the blue loop (Coppola et al. 2013).

The comparison between theory and observations shows that both metal-poor and metal-rich predictions are either brighter (ZAHB) or hotter (RC) than the observed HB and RC stars. We performed a similar comparison using evolutionary prescriptions constructed by assuming an α-enhanced chemical mixture $[\alpha/\mathrm{Fe}] = +0.4$. Data plotted in Fig. 2 show that α-enhanced isochrones and He burning sequences agree quite well with observations. The comparison also indicates that old and intermediate-age He burning stars could be explained with a raw observed peak-to-peak spread in iron abundance of 0.4±0.2 dex. However, the evidence that α-enhanced predictions agree better with observations than scaled-solar ones is at odds with current spectroscopic measurements suggesting that Carina RGs do not show evidence of α-enhancement ($[\mathrm{Ca + Mg + Ti/3Fe}] = 0.06$, Shetrone et al. 2003; $[\mathrm{Ca + Mg + Ti/3Fe}] = 0.07$, Venn et al. 2012).

3. Summary

We compared theoretical prescriptions for He burning phases with Carina accurate multiband photometry (Bono et al. 2010a). The predicted He burning sequences, from BaSTI data base, span from old to intermediate-age progenitors. In particular, we presented the comparison with two metal abundances and two different chemical mixtures (scaled-solar, α-enhanced). We found a satisfactory agreement with the α-enhanced chemical composition $[\alpha/\mathrm{Fe}] = +0.4$, providing a mean metallicity value of $[\mathrm{Fe/H}] \sim -1.8$ with a raw observed peak-to-peak spread in iron abundance of 0.4±0.2 dex.

Acknowledgements. This work was partially supported by PRIN-INAF 2011 "Tracing the formation and evolution of the Galactic halo with VST" (PI: M. Marconi) and by PRINMIUR (2010LY5N2T) "Chemical and dynamical evolution of the Milky Way and Local Group galaxies" (PI: F. Matteucci).

References

Battaglia, G., et al. 2012, ApJ, 761, L31
Bono, G., et al. 2000, ApJ, 543, 955
Bono, G., et al. 2010a, PASP, 122, 651
Bono, G., et al. 2010b, ApJ, 708, L74
Cassisi, S., et al. 2007, ApJ, 661, 1094
Coppola, G., Stetson, P. B., Marconi, M., et al. 2013, ApJ, 775, 6
Dall'Ora, M., et al. 2003, AJ, 126, 197
Fabrizio, M., et al. 2011, PASP, 123, 384
Fabrizio, M., et al. 2012, PASP, 124, 519
Fiorentino, G., et al. 2012, ApJ, 759, L12
Grcevich, J., et al. 2009, ApJ, 696, 385
Lemasle, B., et al. 2012, A&A, 538, A100
Łokas, E. L., et al. 2010, ApJ, 708, 1032
Mateo, M. L. 1998, ARA&A, 36, 435
McCall, M. L. 2004, AJ, 128, 2144
McConnachie, A. W. 2012, AJ, 144, 4
McDonald, et al. 2011, ApJS, 193, 23
Monelli, M. et al. 2003, AJ, 126, 218
Pietrinferni, A., et al. 2004, ApJ, 612, 168
Pietrinferni, A., et al. 2006, ApJ, 642, 797
Pietrzyński, G., et al. 2009, AJ, 138, 459
Rocha, M., et al. 2012, MNRAS, 425, 231
Rocha, M., et al. 2013, MNRAS, 430, 81
Shetrone, M., et al. 2003, AJ, 125, 684
Skillman, E. D. et al. 1989, MNRAS, 240, 563
Small, E. E., et al. 2013, MNRAS, 428, 763
Sweigart, A. V. et al. 1989, ApJS, 69, 911
Stetson, P. B., et al. 2011, The Messenger, 144, 32
Venn, K., et al. 2012, ApJ, 751, 102